Macrophage-specific responses to human- and animal-adapted tubercle bacilli reveal pathogen and host factors driving multinucleated cell formation

Christophe J. Queval[1], Antony Fearns[1], Laure Botella[1], Alicia Smyth[2], Laura Schnettger[1], Morgane Mitermite[2], Esen Wooff[3], Bernardo Villarreal-Ramos[3,4], Waldo Garcia-Jimenez[5], Tiaan Heunis[6], Matthias Trost[6], Dirk Werling[7], Francisco J. Salguero[8], Stephen V. Gordon[2] and Maximiliano G. Gutierrez[1*]

[1]The Francis Crick Institute, UK; [2]UCD School of Veterinary Medicine and Conway Institute, University College Dublin, Ireland; [3]Animal and Plant Health Agency, UK; [4]IBERS, Aberystwyth University, U.K; [5]University of Surrey, UK; [6]Newcastle University, UK; [7]Royal Veterinary College London, UK; [8]Public Health England, UK

[*]Corresponding author: max.g@crick.ac.uk

Abbreviations:

MNCs: Multinucleated Cells; hMϕ: Human Macrophage; bMϕ: Bovine Macrophage; Mtb: *Mycobacterium tuberculosis* H37Rv; Mbv: *Mycobacterium bovis* AF2122/97; EVs: Extracellular Vesicles

Short title:

Mbv-specific extracellular vesicles promote MNCs formation

Key words

Tuberculosis, *Mycobacterium bovis*, *Mycobacterium tuberculosis*, multinucleated cells, bovine macrophages, human macrophages, MPB70, extracellular vesicles, granuloma, host-tropism

Abstract

The *Mycobacterium tuberculosis* complex (MTBC) is a group of related pathogens that cause tuberculosis (TB) in mammals. MTBC species are distinguished by their ability to sustain in distinct host populations. While *Mycobacterium bovis* (Mbv) sustains transmission cycles in cattle and wild animals and causes zoonotic TB, *M. tuberculosis* (Mtb) affects human populations and seldom causes disease in cattle. However, the host and pathogen determinants driving host tropism between MTBC species are still unknown. Macrophages are the main host cell that encounters mycobacteria upon initial infection and we hypothesised that early interactions between the macrophage and mycobacteria influence species-specific disease outcome. To identify factors that contribute to host tropism, we analysed both blood-derived primary human and bovine macrophages (hMϕ or bMϕ, respectively) infected with Mbv and Mtb. We show that Mbv and Mtb reside in different cellular compartments and differentially replicate in hMϕ whereas both Mbv and Mtb efficiently replicate in bMϕ. Specifically, we show that out of the four infection combinations, only the infection of bMϕ with Mbv promoted the formation of multinucleated cells (MNCs), a hallmark of tuberculous granulomas. Mechanistically, we demonstrate that both MPB70 from Mbv and extracellular vesicles released by Mbv-infected bMϕ promote macrophage multi-nucleation. Importantly, we extend our *in vitro* studies to show that granulomas from Mbv-infected but not Mtb-infected cattle contained higher numbers of MNCs. Our findings implicate MNC formation in the contrasting pathology between Mtb and Mbv for the bovine host, and identify MPB70 from Mbv and extracellular vesicles from bMϕ as mediators of this process.

Introduction

Host tropism is determined by the range of host species that a pathogen can infect and transmit between, allowing it to sustain in the host population. *Mycobacterium tuberculosis* (Mtb) causes tuberculosis (TB) in humans and remains the leading cause of morbidity and mortality worldwide from a single infectious agent, with 1.8 million deaths in 2018 [1]. Mtb is an obligate pathogen, with transmission between individuals *via* aerosols. Infection generally occurs in terminal lung airways, where the bacillus is taken up by alveolar macrophages before disseminating to other organs. Regardless of which tissues are involved, the immune response against the

bacillus progressively leads to the formation of granulomas, where the bacilli can either disseminate or persist [2-4].

On the other hand, bovine TB is caused by *M. bovis* (Mbv), that displays a broad host-range, infecting and transmitting between a variety of livestock and wildlife populations [5]. Mbv also poses a risk as a zoonotic pathogen, representing a serious threat to human health [1]. In 2005, the WHO declared bovine TB as the most neglected zoonotic disease threatening human health [6-8].

The genomes of Mbv and Mtb are over 99.9 % identical [9]. The main genomic differences between these two pathogens encompass 8 regions of difference (RDs) and over 2000 single-nucleotide polymorphisms (SNPs) [9, 10]. While this level of genetic difference is relatively small, it results in major phenotypic variation that ultimately defines host tropism. Comparative analysis of the Mbv AF2122/97 and Mtb H37Rv transcriptome and proteome revealed upregulation of 77 and 103 genes and encoded proteins, respectively, in each pathogen [11]. Proteins showing differential abundance included known virulence factors such as EsxA, EsxB as well as the immunogenic MPB70 and MPB83 [11-15].

In both human and bovine TB, macrophages are the first line of defence as well as one of the main cellular reservoirs of tubercle bacilli [16]. Here, we compared two archetypal MTBC host-adapted species, Mtb H37Rv and Mbv AF2122/97 [9, 10, 17] for *in vitro* interactions with monocyte-derived primary human (hMϕ) or bovine (bMϕ) macrophages. We show that Mtb and Mbv reside in different cellular compartments and differentially replicate in hMϕ, while both strains efficiently replicate in bMϕ. We demonstrate that both *in vitro* and *in vivo*, Mbv specifically promotes multinucleated cells (MNCs) formation in bMϕ, arguing that this host-specific MNCs generation contributes to the contrasting pathogenesis between Mtb and Mbv in cattle. Finally, we show that the secreted Mbv protein MPB70 and bMϕ -derived extracellular vesicles (EVs) are bacterial and host factors specifically implicated in bMϕ-multi-nucleation. Our results have identified functional differences between Mbv and Mtb host-pathogen interaction that reveal a role for MPB70 and EVs in the process of multinucleation, a process that may play a crucial role in MTBC host tropism.

Results

Mtb and Mbv differentially replicate within human or bovine macrophages.

In order to identify host and bacterial factors during species-specific macrophage interactions, we set up an experimental infection model comparing, side by side, blood-derived primary human or bovine macrophages (hMϕ and bMϕ, respectively) infected with either Mtb or Mbv. First, we optimized the infection ratios for both macrophage models by analysing the ability of hMϕ and bMϕ to phagocytose Mtb-RFP or Mbv-RFP. After 2 h, we observed that Mtb-RFP and Mbv-RFP uptake was similar in both hMϕ or bMϕ. However, bacterial uptake was approximately 8 to 10 times higher in bMϕ when compared to hMϕ (data not shown). In order to normalize the infection protocol, we then infected bMϕ with a lower MOI (MOI of 1) than hMϕ (MOI of 10) (Fig. S1*A*). We then monitored Mtb and Mbv replication in hMϕ and bMϕ by microscopically quantifying their intracellular growth after 72 h of infection (Fig. 1*A*). In hMϕ, Mtb replicated as previously shown [18] whereas Mbv replication was delayed (Fig. 1*B*). In contrast, both Mtb and Mbv replicated at similar rates in bMϕ up to 72 h (Fig. 1*C*). After 72 h of infection, there was cytotoxicity associated with bMϕ but not hMϕ (Fig. S1*B* and S1*C*). In hMϕ, cytotoxicity was detectable after 5 days of infection with Mtb, while a significant number of hMϕ infected with Mbv was still detectable (Fig. S1*C*). Next, we assessed the cytotoxicity of Mtb in hMϕ using the cell death reporter Green Live/Dead (Fig. S1*D*). After 5 days of infection, Mtb actively replicated in hMϕ and was associated with cell death while Mbv slowly replicated in hMϕ with limited cell death (Fig. S1*D*). We then infected hMϕ at a low MOI (MOI 2) with Mtb-RFP and Mbv-RFP for 8 days and found that Mbv replication significantly increased after 8 days of infection compared to the basal uptake observed 2 h post-infection (Fig. S1*E*). Thus, the progression of Mbv-intracellular replication in hMϕ suggests that, although Mbv replication is restricted compared to Mtb, hMϕ failed to completely eradicate the infection.

Intracellular localization of Mtb and Mbv differs in human macrophages

Next, we tested whether the different bacterial replication rates were associated with a differential ability of Mtb or Mbv to evade host macrophage restriction. Although both hMϕ and bMϕ were produced with a similar method, electron microscopy analysis showed that the cytoplasm of resting bMϕ was strongly enriched with spacious single-membrane vesicles when compared to hMϕ (Fig. S1*F*). These large

vacuoles were positive for the late endosomal marker, LAMP-1 (Fig. S1*G*). Whereas in hMϕ the localisation of intracellular mycobacteria is relatively well characterised [16, 19], the localisation of Mbv in bMϕ is unknown. We therefore quantified the percentage of bacteria associated with (i) the late endosomal marker LAMP-1, (ii) the pH-sensitive Dye Lysotracker Red (LTR) or (iii) the autophagosome marker LC3B, after 24 h of infection (Fig. S2). For that, we used two different approaches to quantify the localisation: one for markers closely associated with bacteria [20] and another method for spacious compartments such as the LAMP-1 positive phagosomes [21]. In hMϕ, 37% ± 14.7 and 39% ± 11.9 of Mtb and Mbv respectively were found associated with LAMP-1. Similarly, in bMϕ, 45% ± 9.4 and 36% ± 5.4 of Mtb and Mbv, respectively, were found in a LAMP-1-positive vacuole. The high level of bacterial association with the LAMP-1 marker suggests that, in both species, a significant fraction of the bacteria is membrane-bound (Fig. S2*A* and S2*B*). In contrast, only 15 to 20% were found associated with lysotracker in both hMϕ and bMϕ, suggesting that, independent of the host species, a limited proportion of membrane-bound mycobacteria were in acidic compartments after 24 h of infection (Fig. S2*C* and S2*D*).

In hMϕ, LC3B was found associated with 28% ± 6.06 of Mbv, while only 10% ± 0.86 of Mtb was positive for this autophagosome marker (Fig. S2*E*). Autophagy is an anti-mycobacteria pathway [22-24] and the higher association of Mbv with LC3B-positive compartments may explain the delayed intracellular replication. However, Mtb and Mbv presented a similar association with LC3B or all the other markers tested in bMϕ (Fig. S2*F*). Next, we analysed the localisation of mycobacteria at the ultrastructural level and defined the proportion of bacteria localised in (i) a single-membrane phagosome, (ii) in a multi-membrane vacuole or (iii) cytosolic (Fig. 1*D* and 1*F*). In hMϕ, circa 40% of the Mtb population was localised in the cytosol. Mtb also resided in a single-membrane compartment (>55%) and a minor proportion in multi-membrane compartments (<5%) (Fig. 1*D* and 1*F*). In contrast, the majority of Mbv were localized in single- and multi-membrane compartments (>75% and around 20%, respectively) and only a minority of Mbv was localised in the cytosol (<5%) (Fig. 1*D* and 1*F*). On the other hand, in bMϕ, the majority of Mtb localised in the cytosol (around 75%) whilst the rest mainly resided in a single-membrane compartment (Fig. 1*F*). Moreover, Mbv was associated with single-membrane compartments and also localised in the cytosol of bMϕ (Fig. 1*F*). Given that cytosolic

DNA will trigger expression of interferon-β (IFNβ) [23, 25, 26], we monitored by RT-qPCR the expression of *IFN-β* in hMϕ and bMϕ infected with Mtb or Mbv. We found that Mtb induced higher *IFN-β* levels than Mbv in hMϕ and bMϕ, confirming that, regardless of species, Mtb accessed the cytosol more efficiently than Mbv (Fig. 1*G*).

Mbv specifically induces the formation of multinucleated cells (MNCs) in bMϕ

The similar features observed for both pathogens during infection of bMϕ did not reflect the attenuated phenotype of Mtb seen in cattle [27]. However, we noticed that the fusogenic properties of bMϕ were different after infection with either Mtb-RFP or Mbv-RFP. As early as 24 h post-infection, bMϕ tended to form multinucleated cells (MNCs) especially when infected with Mbv (Fig. 2*A*). A quantitative analysis of MNCs numbers confirmed that Mbv infection induced more MNCs when compared to Mtb-infected or non-infected (NI) cells (Fig. 2*B*). Multi-nucleation of bMϕ occurred only with live bacteria since paraformaldehyde-killed-Mbv (PFA-*Mbv*) failed to induce MNCs (Fig. S3*A* and S3*B*). This effect was restricted to bMϕ, since MNCs were almost absent in hMϕ infected either with Mtb or Mbv (Fig. 2*C*). At the ultrastructural level, we confirmed that the multiple nuclei were contained in a single cell (Fig. 2*D* and Fig. S3*C*). MNCs were significantly larger than mononucleated bMϕ and contained a central vesicle-rich area surrounded by intact nuclei (Fig. 2*D*). Although the number of nuclei was variable, their circular alignment within the periphery of the cytosol was reminiscent to the morphology of the multinucleated giant cells (also called Langhans' cells) present in granulomatous lesions (Fig. 2*D* and Fig. S3*C*). Altogether, these data suggest that as early as 24 h post infection, Mbv interactions with bMϕ induces the formation of MNCs. Importantly, 54 and 58% of MNCs observed by fluorescence microscopy were uninfected, suggesting a bystander effect (Fig. 2*E* and 2*F*). To test this possibility, we stimulated naïve bMϕ with filtered supernatant from infected-bMϕ. Only supernatants from Mbv-infected bMϕ led to a significant increase in MNCs formation when compared to supernatants from non-infected or Mtb-infected bMϕ (Fig. S3*D*). In agreement with a species-specific phenotype, supernatants from hMϕ infected with either Mtb or Mbv failed to induce multi-nucleation in bMϕ (Fig. S3*D*). These results demonstrate that factors present in the extracellular medium contribute to multi-nucleation in bMϕ. The factor(s) responsible for cell multi-nucleation were proteinaceous since heat-inactivated supernatant did not induce MNCs formation (Fig. S3*D*). Similar experiments in

infected hMϕ showed that none of the conditions tested increased the number of MNCs (Fig. S3*E*). These data show that proteins secreted by bMϕ after infection with Mbv induced MNCs formation.

Secreted bacterial MPB70 contributes to MNCs formation in bMϕ

One of the main differences between Mbv and Mtb is the level of expression of genes in the SigK regulon that encode secreted proteins such as MPB70. The gene encoding MPB70 is highly expressed by Mbv, whereas its expression is low in Mtb *in vitro* but shows intracellular induction [28]. Furthermore, MPB70 contains a FAS1-domain, a structure that is known to play a role in cell adhesion [29, 30]. Hence, we hypothesised that MPB70 induces multinucleation during Mbv macrophage infections [11, 14, 31, 32]. To investigate whether MPB70 affects bMϕ multi-nucleation, we generated an Mbv strain with the gene encoding MPB70 deleted (Mbv ΔMPB70) and the complemented strain (Mbv-Compl) (Fig. 3 and Fig. S4**)**. As expected, deletion of the MPB70 gene completely abolished the secretion of MPB70 in Mbv ΔMPB70 compared to Mbv wild type (Mbv WT) and Mbv-Compl (Fig. 3*A*). Next, we infected bMϕ with Mbv WT, Mbv ΔMPB70 or Mbv-Compl and analysed the numbers of MNCs after 24 h of infection (Fig. 3*B*). We found that the Mbv ΔMPB70 mutant lost its ability to induce multinucleation. In agreement with MPB70 having a role in the multinucleation process, infection with Mbv-Compl induced MNCs formation at similar levels to that of Mbv WT infection (Fig. 3*C*). We concluded that MNCs formation in bMϕ is a specific response to MPB70 activity after Mbv infection.

Extracellular vesicles from Mbv-infected bMϕ promote MNCs formation.

To identify the host factors involved in bMϕ multi-nucleation, we analysed the secretome of Mtb- versus Mbv-infected bMϕ. We identified 1341 host proteins in the cell-free supernatants and found that 192 proteins showed differential abundance between mycobacteria-infected bMϕ and uninfected control samples by mass spectrometry-based proteomics (Fig. 4*A*). Notably, the majority of the identified proteins were associated with extracellular vesicle (EVs) biogenesis and trafficking, cellular focal adhesion or membrane trafficking (Fig. 4*A*). Furthermore, 27 proteins were found to be differentially secreted between Mtb- and Mbv-infected bMϕ (Fig. 4*B* and 4*C***,** Table S1). Given the marked presence of EVs-associated signature in the proteomic analysis, we hypothesized that EVs released during infection might

contribute to the bMϕ multi-nucleation. To test this, we isolated EVs and assessed the quality and purity of the EVs-enriched fractions by electron microscopy (Fig. 4*D* and 4*E*). Naïve bMϕ were then stimulated for 24 h with the EVs-enriched fraction from uninfected (NI), Mtb- or Mbv- infected bMϕ, or with serum-free medium (SFM) as a negative control. The percentage of MNCs significantly increased in bMϕ stimulated with the EVs fraction from Mbv-infected bMϕ, whereas the EVs from Mtb-infected bMϕ did not induce MNCs formation (Fig. 4*F* and 4*G*). Altogether, our data suggest that Mbv-induced EVs contribute to bMϕ multi-nucleation by acting as cargo for the transport and delivery, to targeted cells, of key components involved in the multi-nucleation process.

Granulomas from Mbv-infected cattle contain a higher number of MNCs than Mtb-infected cattle.

Inflammation occurring within granulomatous lesions leads to the formation of specific multinucleated cells called Langhans' cells. Our *in vitro* data suggested that cattle infected with Mbv or Mtb should show variation in Langhans' cells *in vivo*. Post-mortem histopathological analysis was performed on H&E stained thoracic lymph node (LN) sections from cattle infected with Mtb H37Rv for 10 weeks or with Mbv AF2122/97 for 6 weeks. Limited numbers of granulomas were detected in LNs from cows infected with Mtb (Fig. 5). In agreement with previously described studies [27, 33], Mtb-induced granulomas were at an early stage of maturation (type I and II as described by [34, 35]), with limited traces of necrosis or caseification (Fig. 5*A* and 5*C*). In contrast, LNs from cows infected with Mbv contained a large number of granulomatous lesions at all stages of maturation (Fig. 5*B* and 5*C*).

In agreement with the *in vitro* data, we found that the number of MNCs present in Mtb-induced granulomas was significantly lower than in Mbv-induced granulomas (Fig. 5*A*, 5*B* and 5*E*). It is noteworthy that for a similar amount of Acid Fast-positive Bacilli (AFB) detected in stage II granulomas from both Mtb- and Mbv-infected cows (Fig. 5*D*), Mbv-infected granulomas contained around 2.5 times more MNCs compared to Mtb-infected granulomas (Fig. 5*E*). Moreover, the number of MNCs increased during granuloma maturation, suggesting that the expansion of the MNCs population correlates with the severity of granulomatous inflammation.

Discussion

In this work, by analysing infections of Mϕ from two host species with two host-adapted mycobacteria, we shed new light on species-specific host-pathogen interactions in tuberculosis. When comparing the Mϕ infections side-by-side, unexpectedly, there were no striking species-specific differences in bacterial replication that could explain host tropism in human and bovine TB. Mtb replicates more efficiently than Mbv in hMϕ, while both pathogens replicated similarly in bMϕ. These differences could be related to the differentiation protocols and more studies are needed to identify the possible differentiation factors implicated. Nevertheless, both Mtb and Mbv showed similar uptake in each Mϕ species, suggesting that despite the interspecies differences, both Mtb and Mbv are similarly recognized by macrophage receptors.

Mtb produces MNCs in human disease and animal models, but the underlying mechanisms remain unclear. Here we show that both *in vitro* and *in vivo* the specific interaction between Mbv and the bovine host led to the formation of MNCs, arguing that both host and pathogen factors are required for MNC formation. Because the production and secretion of the mycobacterial protein MPB70 is one of the main phenotypic differences between Mbv and Mtb [14], this protein was an obvious candidate. Moreover, MPB70 has homology with the cell adhesion domain Fasciclin 1 (Fas1), Osteoblast-specific factor II (OSFII) or βIgH3, suggesting that MPB70 could mediate cell-to-cell contact or cellular adhesion by interacting with cellular receptors such as stabilins, integrins, as well as extracellular matrix components [29, 30]. Cell-adhesion is a crucial step in the fusion process, bringing Mϕ into close contact with extracellular matrix components. It is tempting to speculate that MPB70 is implicated in bMϕ fusion by mediating cellular interactions and adhesion properties. The differential expression of MPB70 between both pathogens may also partially explain the inability of Mtb to induce MNCs in our *in vitro* model. On this latter point, further studies are needed to explore the kinetics of MNC formation in vitro and if, or how, Mtb can be modified to induce bMϕ MNC formation. Although MPB70 expression is low in Mtb, its expression may increase in stress conditions such as exposure to antibiotics or depending on the Mϕ lineage in which the pathogen resides [36, 37]. The MPB70 homologous protein MPT70 is thus likely secreted by *M. tuberculosis* and locally accumulates during human TB progression, contributing to the formation

of MNCs in human TB. The observed reduced levels of MNCs in granulomas from cattle infected with Mtb as compared to Mbv further indicates that multinucleation requires both host and pathogen factors.

Our results that bMϕ multi-nucleation is driven by factors released into the extracellular milieu after infection suggested a host factor was also involved. In this context, the extracellular microenvironment plays an important role in Mϕ fusion and MNC-formation. The cell density, the nature of the extracellular matrix, and the local concentration of growth factors, chemokines or cytokines are important factors for cell differentiation, cell-to-cell contact and membrane fusion [38-40]. In agreement with this notion, the Mbv-infected bMϕ secretome analysis revealed a dominant signature of proteins related to cell-adhesion, membrane trafficking, and extracellular vesicles. Extracellular vesicles and exosomes play a crucial role in cell communication, inflammation, and are implicated in multiple infectious diseases [41]. During Mtb infection, extracellular vesicles participate in the inflammation process through the recruitment of Mϕ to the site of infection, the modulation of immune responses, antigen presentation, and/or transport of bacterial components [42-45]. Exosomes from murine J774 macrophages infected with Mtb contained several antigenic bacterial proteins such as EsxA, EsxB, SapM, PknG as well as MPB32, MPB53, MPB63 and MPB64 [42]. We speculate that EVs modulate cell multinucleation by acting as cargo for the transport of host and bacterial factors that will promote multi-nucleation. In our proteomics approach, we were not able to detect Mtb proteins and complementary approaches with increased sensitivity are needed for the identification of bacterial factors present in the supernatants. *In vivo*, when released, these vesicles may then traffic towards the tissue to another site such as the periphery of granulomas, interact with resident macrophages and promote the formation of MNCs.

During TB inflammation, macrophage fusion occurs during granuloma progression leading to MNCs or Langhans' cells. Generally, Langhans' cells are localised at the peripheral epithelioid rim of the granuloma and can contain around 20 nuclei. Langhans cells, associated with granulomatous lesions, are derived from pro-inflammatory macrophages (CD68+, CD40+, DC-STAMP+), which fuse in response to inflammatory stimuli such as macrophage-colony stimulating factor (M-CSF), Tumour necrosis factor-α (TNF- α) or interferon-γ (IFN- γ) [46-49]. Although the role of MNCs in the granuloma is still unclear, several studies suggest a role of these

cells in inflammation and bacterial control (reviewed in [46, 50]). MNCs can indeed take up large targets for degradation [51] and when they mature and lose their ability to uptake bacteria, the remaining NADH oxidase activity and antigen presentation clear all pathogens already inside [52].

Mtb has previously been isolated from lesions found in naturally infected cattle [53-56]. These latter cases show that, in certain circumstances, Mtb can cause disease in cattle, an outcome that may depend on the genetic background of both the infecting strain and host, as well as immune status. This underlines the need to unravel the mechanistic basis for MNC formation in well controlled experimental systems. In a head to head experimental cattle infections, we have previously shown that two Mtb strains, the hallmark H37Rv and an Mtb isolated from a bull in Ethiopia (BTB1558) are attenuated in cattle as compared to Mbv AF2122/97, with the latter inducing greater inflammation and pathology [11, 27]. Here we found that, even when the amounts of bacteria are comparable, Mbv induces a much higher number of MNCs per granuloma than Mtb, including the early stage type I and type II granulomas. This suggests that the intensity of the inflammatory response *in vivo* influences not only granuloma maturation but also the formation of MNCs. Reduction of inflammation by treatment with anti-inflammatory IL-10 has been shown to reduce both granulomatous inflammation and MNCs formation [57]. Additionally, assessment of cytokine expression of MNCs in cattle infected with Mbv showed a correlation between the expression of pro-inflammatory cytokines and the severity of granulomatous lesions [58]. The higher presence of MNCs in Mbv thus correlates with its virulent phenotype in cattle, suggesting a role for MNCs in inflammation, granuloma maturation and severity of TB lesions.

Altogether, our data provide evidence that a combination of bacterial effectors and species-specific responses shapes the singular interaction of the pathogen with its host, in this instance triggering the formation of MNC, one of the cellular hallmarks of granulomas.

Methods

Reagents and antibodies

Recombinant human Granulocyte-Macrophage Colony Stimulating Factor (GM-CSF) and bovine GM-CSF were provided by Miltenyi (#130-093-867) and Abcam (#ab209168), respectively. Dapi used to stain cell nuclei was purchased from Sigma-

Aldrich (#D9542) and the Alexa Fluor-488 Phalloidin was from Invitrogen #A12379. Detection of cell death was visualized using Live/Dead Green dye (ImmunoChemistry #6342). Immunolabelling of LC3B and LAMP-1 was performed using a rabbit anti-LC3B from Enzo Lifesciences (MBL-PM036) and a rabbit anti-LAMP-1 from Abcam (Ab24170). Mouse antibody to MPB70 (#LAB-0007a2) and the Mouse antibody to Ag85 (#ab36731) were purchased from Lionex GmbH and Abcam, respectively. The secondary antibodies used in this study were: goat anti-rabbit conjugated with Alexa Fluor 488 (#A11034), (ii) goat anti-mouse conjugated with Alexa Fluor 488 (#A11029), both purchased from Life technologies and (iii) an anti-mouse conjugated with HRP (#W402B) from Promega. For light or electron microscopy, cells were fixed using Paraformaldehyde (PFA) from Electron Microscopy Sciences (#15710) or Glutaraldehyde from Sigma-Aldrich (#G5882), respectively.

Mycobacterial strains

In the study, we used the sequenced and annotated *M. tuberculosis* H37Rv (Mtb) and *M. bovis* AF2122/97 (Mbv) reference strains as models [9, 10, 17]. Fluorescent Mtb and Mbv were engineered to constitutively express Red fluorescent proteins (RFP) encoded by the plasmid pML2570 integrated into the bacterial genome (Integrase: Giles, Resistance: Hygromycin). Mbv wild type (WT), Mbv *mpb70* knock-out *(*Mbv ΔMPB70) and the Mbv ΔMPB70 complemented strains (Mbv-compl) were used in this study. Mbv ΔMPB70 cloning and complementation are detailed in the paragraph “Cloning and characterisation of *Mycobacterium bovis* 2122/97 *mpb70* knock-out and complemented strains”. Mtb strains were grown in 7H9 Middlebrook broth supplemented with 10% Albumin Dextrose Catalase (ADC), 0.05% Tween 80 and 0.5% glycerol. All Mbv strains were grown in 7H9 Middlebrook supplemented with 10% ADC, 0.05% Tween 80 and 40 mM Sodium Pyruvate. When required, selective antibiotics were added to the medium.

Strains	plasmids	Genetic feature	Selective antibiotic
H37Rv-RFP	pML2570	RFP	Hygromycin 50µg/ml
M.bovis AF2122/97-RFP	pML2570	RFP	Hygromycin 50µg/ml
M. bovis wild-type	None	Wild-type	None
M. bovis ΔMPB70	phAE159	*mpb70* deletion	Hygromycin 50µg/ml

M.bovis ΔMPB70/MPB70 (Mbv-Compl)	phAE159 pEW70c2	*mpb70* deletion pEW70c2-mpb70 complementation	Hygromycin 50 µg/ml Kanamycin 25 µg/ml

Cloning and characterisation of *Mycobacterium bovis* 2122/97 *mpb70* knock-out and complemented strains

Cloning strategy

A knockout mutant in the *mpb70* gene (*Mb2900*) of *M. bovis* 2122/97 was constructed using the phAE159 shuttle phasmid. One kb regions flanking the chromosomal *M. bovis mpb70* were cloned into phAE159 so as to flank a hygromycin resistance marker to generate the allelic exchange substrate (Fig. S4*A*). After amplification in *M. smegmatis* mc2155, recombinant phages were used to infect *M. bovis* wild type and hygromycin resistant Mbv ΔMPB70 transductants were selected. In the deletion mutant complementation was achieved by expression of the wild type *mpb70* gene from the replicating plasmid pEW70c2 (Mbv ΔMBP70::MBP70).

Selection and characterisation by PCR

For PCR analysis, the bacteria were grown in 7H9 media containing 50 µg/ml hygromycin for Mbv ΔMPB70 cultures, and 50 µg/ml hygromycin and 25 µg/ml kanamycin for Mbv-Compl cultures. DNA for PCR analysis was collected through crude DNA extraction. PCRs were performed with the Phusion High-Fidelity DNA polymerase from NEB, using the Phusion GC Buffer. The primers listed below were used to ascertain the presence of *dipZ* and/or *mpb70* genes (Fig. S4*B* and S4*C*) List of primers: *dipZ*-Forw: GAATTACCACGCCAAAGACG; *dipZ*-Rev: TCATCCGTAGGTGAAGGAAAA; *dipZ-mpb70*-intergenic-Forw: GCTCCGAAGAAATCATGTCG; *mpb70*-5'end-Rev: AGACAGCCACCGCCAGAG; *mpb70*-Rev: CTGCGACATTCCCTGCAC.

Detection of secreted MPB70 by Western blot

The bacteria were grown in Sauton's media with antibiotics added as appropriate (described above). The supernatant of each strain was collected and concentrated with Amicon Ultra-15 Centrifugal Filter Units. Protein concentrations were then determined using a Pierce BCA Protein Assay kit and the supernatants were diluted to get a normalised whole protein load per well for gel electrophoresis of 25 µg. After

transfer of the proteins to the membrane, the membrane was probed using a mouse anti-MPB70 IgG, and an anti-mouse HRP-conjugated (Fig. S4*D*).

Isolation of primary human and bovine monocytes and differentiation into macrophages

Human monocytes were obtained from leukocyte enriched blood fractions from healthy adult donors provided by the British National Health Service (NHS) under strict anonymity. Bovine blood was obtained from clinical healthy Holstein cows in mid-lactation phase housed at Bolton Park's Farm of the Royal Veterinary College (University of London). Blood was collected by jugular venepuncture into sterile glass bottles containing 10% Acid Citrate Dextrose (ACD) as anticoagulant, as previously described [59]. Prior to monocyte isolation, bovine whole blood was aliquoted into 50 mL centrifugation tubes and centrifuged for 15 minutes at 1200 x*g* to collect the buffy coat. Both human leucocyte enriched fraction and bovine buffy coat were then processed in the standard way but with the difference that PBS-EDTA was used as the buffer for the isolation of human monocytes, while PBS was used for the processing of bovine blood. Peripheral Blood Monocytes Cells (PBMCs) were isolated by centrifugation onto a Ficoll gradient. PBMCs were then washed and CD14-expressing monocytes were labelled with the anti-human CD14-antibody conjugated with magnetic beads (Miltenyi #130-050-201) and isolated by direct magnetic selection using the LS column (Miltenyi #130-042-401). Human and bovine CD14-positive monocytes were finally incubated in RPMI 1640 medium (Gibco # 72400021) containing: GlutaMax, 25 mM Hepes, 10% Foetal bovine serum (FBS) and 10 ng/mL of recombinant human GM-CSF or 20 ng/mL of recombinant bovine GM-CSF to allow differentiation into Mϕ for 7 days at 37˚C in an atmosphere containing 5% CO_2.

Cell culture

After 7 days of differentiation, when Mϕ were ready for infection and during all the infection process, GM-CSF was omitted from the culture medium. Once differentiated, MΦ were washed once with PBS and detached from the petri dish by incubation for 20 min at 4˚C in PBS-EDTA followed by gentle scrapping. Cells were

seeded depending on the type of experiment. For immunofluorescence, $1.8x10^5$ cells/well were seeded into 24 well plates containing untreated glass coverslips (diameter 10 mm, No:1.5). For stereology, electron microscopy, transfer supernatant assays or RT-qPCR, cells were seeded into 6 well plates at a concentration of $7x10^5$ cells/well. Alternatively, untreated glass bottom (No:1.5) dishes with grids from Matek Corporation (#P35G-1.5-14-C-GRID) containing $2x10^5$ cells/dish were used for light and electron microscopy.

Mycobacteria preparation and macrophage infection:

Bacterial strains were cultured in a 50 mL centrifugal Falcon tube containing their respective optimal media until the exponential phase was reached. One day before infection, bacteria were diluted to reach an Optical Density (OD_{600nm}) of 0.4 and cultured for an additional 24 h. Prior to infection, bacteria were pelleted by centrifugation at 2,900 xg for 5 min and washed twice with PBS. Bacteria were pelleted again before adding an equivalent number of sterile 2.5- to 3.5-mm glass beads that matched the pellet size into the Falcon tube (usually 4–5 beads). The Falcon tubes were then vigorously shaken for 1 min to break up bacterial clumps. The bacteria were suspended in 7 ml of RPMI 1640 medium containing GlutaMax, 25 mM HEPES, 10% FBS (complete RPMI) and transferred to a 15 mL centrifugal Falcon tube. Bacterial suspensions were then spun down at low speed (150 xg) for 3 min to allow the removal of the remaining bacterial clumps. The supernatant, cleared of bacterial clumps, was transferred into a clean 15 mL Falcon tube and the OD_{600nm} was measured to determine the concentration of the bacterial suspension, and further diluted in complete RPMI to reach a final OD_{600nm} of 0.1 (based on growth curves it was determined that an OD 0.1 the density of bacteria in the culture is 1×10^7 bacteria/ml; data not shown). Bacteria were finally added to the MΦs at an MOI of 10 for hMϕ infection or an MOI of 1 for bMϕ infection and incubated at 37˚C in an atmosphere containing 5% CO_2 for 2h (bacterial uptake). Cells were then washed twice with PBS, the medium was replaced with fresh complete RPMI and incubated at 37˚C in an atmosphere containing 5% CO_2 until the samples were processed for analysis.

Supernatant stimulation assay

Human or bovine Mϕ were seeded into 6 well or 24 well plates and infected as described above. The supernatants were then collected, sterilized by double filtration using 0.22 µm PVDF filters, before being transferred onto naïve uninfected Mϕ. Supernatant-stimulated Mϕ were then incubated for 24 h at 37˚C in an atmosphere containing 5% CO_2. For each experiment, infected Mϕ and supernatant-stimulated Mϕ were from the same donor. Finally, Mϕ were fixed overnight with a solution of PBS-PFA 4% before being stained for immunofluorescence.

Extracellular vesicle (EVs) purification

Two and a half million of bMϕ were seeded into T25 cm^2 flasks and incubated in complete RPMI, overnight at 37°C in an atmosphere containing 5% CO_2. The following day, cells were infected with Mtb-RFP or Mbv-RFP at an MOI of 2. After 2 hours uptake, cells were washed 3 times with PBS to remove bacteria and residual FBS. Cells were then fed with RPMI 1640 without FBS (5 mL per T25 cm^2 flask) and incubated 24 hours at 37°C in an atmosphere containing 5% CO_2. After 24 h infection, the supernatant from two T25 cm^2 flasks (total volume of at least 10 ml) was collected and processed for EVs purification using the Exo-spin purification Kit from Cell guidance systems (#EX01). Briefly, the supernatants were cleared by ultracentrifugation at 16,000 xg for 30 minutes. Ten mL of cleared supernatants were then mixed with 5 mL of Exo-spin buffer and incubated overnight at 4°C. EVs were then precipitated by centrifugation at 16,000 xg for 90 min. EVs pellets were then suspended in PBS and purified using a size exclusion chromatography resin column. A small fraction of EVs were fixed with PBS-Glutaraldehyde 1% and PFA 4% solution and purity control was assessed by Electron microscopy. The rest of EVs-enriched fractions were finally diluted in complete RPMI and used to stimulate naïve bMϕ. After 24 h of stimulation with EVs, cells were fixed with PBS-PFA 4% solution and the number of MNCs was assessed by confocal light microscopy.

Immunofluorescence and image acquisition

Immunofluorescence

Cells were cultured onto glass coverslips. Prior to immunolabeling, cells were fixed overnight at 4°C with a PBS-PFA 4% solution. Fixed cells were then incubated for 10 min at room temperature (RT) with a solution of PBS-NH_4Cl 50 mM to quench free aldehyde groups, before being permeabilized for 20 min with PBS-Saponin 0.2%. Cells were then blocked for 30 min with PBS-BSA 1%. For the immunofluorescence,

both primary and secondary antibodies were diluted in PBS-Saponin 0.02%-BSA 0.1% (dilution buffer). LC3B and LAMP-1 were labelled using a rabbit anti-LC3 (dilution 1/200) and a mouse anti-LAMP-1 (dilution 1/100). After 1 h incubation at RT, cells were washed three times with PBS and incubated with the respective secondary antibodies for one additional hour. Cells were washed 3 times prior to nuclei staining with DAPI. When required, the actin cytoskeleton was labelled using phalloidin conjugated with Alexa-Fluor 488 (dilution 1/800 into dilution buffer; incubation 45 min at RT). For the detection of live versus dead cells, the cells were stained with Green Live/Dead stain (500 nM for 10 min at RT) prior to PFA fixation. The coverslips were finally mounted onto microscopy glass slides using Dako fluorescence mounting medium (Dako, #S3023).

Image acquisition

Confocal images were acquired using a confocal inverted microscope (Zeiss LSM710) or Zeiss LSM880 both equipped with a 40X oil Lens or Plan-Apochromat 63x/1.4 NA lens and excitation laser 405, 488, 561, 633 nm. For the quantification of multinucleated cells, a field was randomly chosen and images were acquired in tile scan mode (4x4) with 40X oil lens.

Image analysis

Image analysis was performed using free open-source FIJI software (NIH). Zeiss LSM confocal images files (.czi) were opened using the BioFormats plug-in of FIJI.

Cell number and intracellular bacterial growth

Confocal images were first split into separate channels: Cell nuclei DAPI (blue), RFP (red) corresponding to RFP-mycobacteria.

(a) To measure the number of cells, a threshold was applied to the DAPI images in order to mask and calculate the number of nuclei. The presence of multinucleated cells in the field was manually adjusted for each image. (b) The bacterial area was calculated by applying the threshold function in the RFP-channel to mask the fluorescent bacteria. “Analyse Particles” function of FIJI (size = 0.5–infinity, circularity = 0–1) was applied to calculate the area of each bacteria. For each time point, the intracellular growth was expressed in bacteria (RFP) area per cell.

Intracellular markers association

Confocal images were first split into separate channels: Cell nuclei DAPI (blue), RFP-mycobacteria (red) and Green channel corresponding to the marker tested

(e.g., LC3B). The cell number and bacteria area were determined as described in (a) and (b). Mask corresponding to all the bacteria was created and each bacteria object was extended from 2 pixels using the function “Dilate” and converted into a “region of interest”. Finally, the green channel corresponding to the cellular marker was subjected to pixel intensity measurement within the bacteria region of interest. Marker association was expressed in mean intensity of green pixels for each bacteria object. For each marker, the fluorescence background was measured from several fields and bacteria were considered positive when the mean intensity of the marker > background + 1 STD. The percentage of association was calculated as follows: number of positive bacteria x 100 / total number of bacteria. All values were analysed and plotted using Excel and GraphPad Prism.

Electron Microscopy

Extracellular vesicle negative staining

Ten µl of sample was incubated at RT on a 200 mesh formvar/carbon grid. Grids were then washed 5 x 1 min in 200 mM HEPES (Sigma-Aldrich H0887) and transferred to 20 µl 1% Uranyl acetate, (UA) (Agar scientific AGR1260A) and incubated for 1 min at RT. Excess 1% UA was removed and the grids were left to dry before imaging. Images were acquired using a 120 kV Tecnai G2 Spirit BioTwin (FEI company) with an Orius CCD camera (Gatan Inc.)

Stereology

Transmission electron microscopy sample preparation for stereology: Cells were washed in PBS and then fixed in 2.5% GA in 200 mM HEPES pH7.4 for 30 min at RT, followed by overnight fixation at 4°C. After several washes in 200 mM HEPES buffer, samples were processed in a Pelco Biowave Pro (Ted Pella, USA) with the use of microwave energy and vacuum. Briefly, samples were fixed and stained using a reduced osmium, thiocarbohydrazide, osmium (ROTO)/en bloc lead aspartate protocol. Samples for stereological analysis were dehydrated using an ethanol series of 50, 75, 90 and 100% then lifted from the tissue culture plastic with propylene oxide, washed 4 times in dry acetone and transferred to 1.5 ml microcentrifuge tubes. Samples were infiltrated with a dilution series of 50, 75, 100 % of Ultra Bed Low Viscosity Epoxy (EMS) resin to acetone mix and centrifuged at 600 xg between changes. Finally, samples were cured for a minimum of 48 h at 60°C before trimming and sectioning. Sectioning and imaging: ultrathin sections (~50nm) were cut with an

599 EM UC7 Ultramicrotome (Leica Microsystems) using an oscillating ultrasonic 35º
600 diamond Knife (DiaTOME) at a cutting speed of 0.6 mm/sec, a frequency set by
601 automatic mode, and a voltage of 6.0 volts. Images were acquired using a 120 kV
602 Tecnai G2 Spirit BioTwin (FEI company) with an Orius CCD camera (Gatan Inc.)
603 Stereological analysis of Mtb infected cells: At least 22 different infected cells per
604 group were imaged at a magnification of 3,900 by systematic and random sampling.
605 Cross points of the stereological test grid over bacteria were counted with regard to
606 the subcellular localization of bacteria, which was determined from images taken at a
607 minimum magnification of x16,000. The following criteria were employed for the
608 assessment of subcellular membrane involvement: (a) Single surrounding
609 membrane; bacteria were, at least partially, tightly lined by a phospholipid bilayer,
610 representing the phagosomal membrane (b) cytosolic; bacteria were surrounded by
611 ribosomes, representing the cytoplasm with no indication of the phagosomal
612 membrane; (c) Multiple surrounding membranes; bacteria were enveloped by double
613 or multiple membrane structures. Data are shown as the proportions of the total
614 counts per sample group.
615
616 **Real-time polymerase chain reaction (RT-qPCR)**
617 hMϕ and bMϕ were seeded into 6 well plates (8 x 10^5 cells per well) and infected as
618 described earlier. Cells were washed three times with PBS before being lysed in
619 Trizol (1 mL per well). mRNAs were purified using Direct-zol RNA Miniprep kit from
620 Zymo Research (#R2052), following the manufacturer's recommendations and
621 reverse transcribed to cDNA with QuantiTect™ Reverse Transcription Kit (Qiagen).
622 Quantitative real-time RT–PCR (qRT–PCR) was performed using 11.25 ng cDNA per
623 well with 0.5 µl TaqMan™ Gene Expression Assay probe and 5 µl
624 TaqMan™Universal PCR Master Mix in a 10-µl reaction volume on an Applied
625 Biosystems™ QuantStudio™ 7 Flex Real-Time PCR System. Each reaction was
626 performed in triplicate. Data was analysed using ExpressionSuite for QuantStudio™
627 (Applied Biosystems). Fold change was determined in relative quantification units
628 using GAPDH for normalization of RT-qPCR. TaqMan probes used were from
629 Thermo Scientific: human *IFN B1*-FAM (Hs01077958-s1), human *GAPDH*-FAM
630 (Hs02786621-g1), bovine *IFN B1*-FAM (Bt03279050-g1) and bovine *GAPDH*-FAM
631 (Bt03210913-g1).
632

Secretome analysis of mycobacterial-infected bovine macrophages

Sample preparation

BMϕ were seeded into 6 well plates and infected with Mtb or Mbv as described above. Uninfected cells were used as control. After 2 h of bacterial uptake, cells were washed three times with PBS and incubated in RPMI 1640 supplemented with glutamine but without FBS and without Phenol Red for 22 h. The supernatants (2 mL) were then collected and sterilized by double filtration using 0.22 µm PVDF filters. Supernatants were then placed at -80°C prior to being analysed.

Filter-aided sample preparation and trypsin digestion of protein samples

Samples were processed using a modified version of the filter-aided sample preparation (FASP) [60]. Briefly, 800 µl of cell-free supernatant was denatured in 4 M urea in 50 mM triethylammonium bicarbonate buffer (TEAB) and loaded onto a 0.5 ml Amicon ultra 30 kDa cut-off spin filter (Millipore). Samples were centrifuged at 12,000 xg for 15 min. Filters were washed thrice/twice by addition of 400 µl UB buffer (8 M urea in 50 mM TEAB) followed by centrifugation (12,000 xg, 15 min). This process was repeated twice for a total of three UB washes. Samples were reduced with 5 mM tris (2-carboxyethyl) phosphine at room temperature for 1 h and subsequently alkylated with 10 mM iodoacetamide for 1 h in the dark. Filters were then washed consecutively thrice/twice by addition of 400 µl UB buffer and twice by addition of 400 ul of TEAB followed by centrifugation (12,000 xg, 15 min). This process was repeated twice for a total of three UB washes. Four hundred µl of TEAB 50 mM was added to each filter, and the samples were centrifuged (12,000 xg, 15 min). This was repeated twice for a total of three TEAB washes.

Proteins were on-filter for 24 h at 37 °C using 200 ng trypsin in a humidified chamber. The filter unit was placed in a new collection tube after digestion, and the peptides were obtained in the flow-through by centrifugation (12,000 xg, 15 min). Peptides were eluted once more from the filter unit by the addition of 250 µl 50mM TEAB and further centrifugation (12,000 xg, 15 min). Trypsin digestion was stopped with the addition of trifluoroacetic acid (TFA) at a final concentration of 1%, and peptides were desalted using Macro C18 Spin Columns (Harvard Apparatus). Peptides were dried before storage at -20 °C.

Mass spectrometry

Peptides were dissolved in 2% acetonitrile containing 0.1% TFA, and each sample was independently analysed on an Orbitrap Fusion Lumos Tribrid mass

spectrometer (Thermo Fisher Scientific), connected to an UltiMate 3000 RSLCnano System (Thermo Fisher Scientific). Peptides were injected on an Acclaim PepMap 100 C18 LC trap column (100 µm ID × 20 mm, 3µm, 100Å) followed by separation on an EASY-Spray nanoLC C18 column (75 ID µm × 500 mm, 2µm, 100Å) at a flow rate of 300 nL/min. Solvent A was 0.1% formic acid, 3% dimethyl sulfoxide in water, and solvent B was 0.1% formic acid, 3% dimethyl sulfoxide, 20% water in acetonitrile. The gradient used for analysis was as follows: solvent B was maintained at 3% for 5 min, followed by an increase from 3 to 35% B in 99 min, 35-90% B in 0.5 min, maintained at 90% B for 5 min, followed by a decrease to 3% in 5 min and equilibration at 3% for 10 min. The Orbitrap Fusion Lumos was operated in positive ion data-dependent mode for Orbitrap-MS and Ion trap-MS2 data acquisition. Data were acquired using the Xcalibur software package. The precursor ion scan (full scan) was performed in the Orbitrap in the range of 400-1600 m/z with a nominal resolution of 120,000 at 200 m/z. Ion filtering for Ion trap-MS2 data acquisition was performed using the quadrupole with a transmission window of 1.6 m/z. The most intense ions above an intensity threshold of 5 x 10^3 were selected for high-energy collisional dissociation (HCD). An HCD normalized collision energy of 30% was applied to the most intense ions, and fragment ions were analysed in the Ion trap using Rapid scan rate. The number of Ion trap-MS2 events between full scans was determined on-the-fly to maintain a 3 sec fixed duty cycle. Dynamic exclusion of ions within a ±10 ppm m/z window was implemented using a 35 sec exclusion duration. An electrospray voltage of 2.0 kV and capillary temperature of 275°C, with no sheath and auxiliary gas flow, was used. The automatic gain control (AGC) settings were 4 × 10^5 ions with a maximum ion accumulation time of 50 ms for Orbitrap-MS, and 1 × 10^4 ions with a maximum ion accumulation time of 45 ms for Ion trap-MS2 scans, respectively. Ions with <2+ or undetermined charge state were excluded from MS2 selection.

Mass spectrometry data analysis

All tandem mass spectra were analysed using MaxQuant 1.6.1.6 [61], and searched against the *Bos taurus* proteome database (containing 23,965 entries) downloaded from Uniprot on 01 December 2018. Peak list generation was performed within MaxQuant and searches were performed using default parameters and the built-in Andromeda search engine [62]. The enzyme specificity was set to consider fully tryptic peptides, and two missed cleavages were allowed. Oxidation of methionine,

N-terminal acetylation and deamidation of asparagine and glutamine was allowed as variable modifications. Carbamidomethylation of cysteine was allowed as fixed modification. A protein and peptide false discovery rate (FDR) of less than 1% was employed in MaxQuant. Proteins were considered confidently identified when they contained at least one unique tryptic peptide. Proteins that contained similar peptides and that could not be differentiated based on tandem mass spectrometry analysis alone were grouped to satisfy the principles of parsimony. Reverse hits, contaminants and protein groups only identified by site were removed before downstream analysis. A label-free quantification strategy was employed using the MaxLFQ algorithm [63] within MaxQuant. Assigned LFQ values of protein groups containing ≥2 unique peptides were used for statistical analysis in Perseus 1.6.2.3 [64]. Data were $\log_2$ transformed and filtered to contain at least two valid LFQ values in one group for comparison. Missing values were imputed using random numbers drawn from a normal distribution that simulates signals from low abundance proteins. An analysis of variance (ANOVA) as performed, and p-values were corrected for multiple hypothesis testing using the Benjamini-Hochberg FDR method. A Tukey's post-hoc test was performed to determine pairwise comparisons among means of the different groups. A total of 192 differentially regulated proteins were identified using an ANOVA and Tukey's post-hoc test. Among those hits, 27 were differentially regulated between H37Rv and *M. bovis* groups.

Data availability

Mass spectrometric raw data has been uploaded to the ProteomExchang. Project accession: PXD017949 (Username: reviewer65235@ebi.ac.uk Password: 5yBTVK8y, Table S2).

Cattle infection and histopathological analysis

Cattle infection

Lymph node tissue samples used in this study were collected from animals infected in the context of a prior study [27]. Cattle had been infected with *Mtb* H37Rv for 10 weeks or *Mbv* AF2122/97 for 6 weeks at the 'Platform for experimentation on infectious diseases' biocontainment level 3 suites of the Institut National de la Recherche Agronomique (INRA) of Tours, France, as previously described [27, 65]. Briefly, eight female Limousin x Simmenthal cattle of approximately six months of

age were divided into two groups of four. Animals were sedated with xylazine (Rompun® 2%, Bayer, France) according to the manufacturer's instructions (0.2 mL/100 kg, IV route) prior to the insertion of an endoscope through the nasal cavity into the trachea for delivery of the inoculum through a 1.8 mm internal diameter cannula (Veterinary Endoscopy Services, U.K.) above the bronchial opening to the cardiac lobe and the main bifurcation between left and right lobes. For each strain, an infective dose of 1×10^4 CFU was delivered endo-bronchially in 2 ml of 7H9 medium. Two ml of PBS were used to rinse any remains of the inoculum into the trachea and then cannula and endoscope were withdrawn. The canal through which the cannula was inserted into the endoscope was rinsed with 20 ml of PBS and the outside of the endoscope was wiped with sterilizing wipes (Medichem International, U.K.) prior to infection of the next animal. Inoculation with the two different pathogens occurred at different days; the endoscope was sterilised as recommended by the manufacturer between the two the infections. Retrospective counting of the inocula revealed infection with 1.66×10^4 CFU Mtb H37Rv and 1.12×10^4 CFU Mbv AF2122/97.

Histopathological analysis

Animals inoculated with Mtb H37Rv or Mbv AF2122/97 were sacrificed 10 weeks or 6 weeks post-infection, respectively and subjected to post-mortem analysis. In this study, tissues evaluated for gross pathology included the following, lymph nodes: left and right parotid, lateral retropharyngeal, medial retropharyngeal, submandibular, caudal, cranial mediastinal and cranial tracheobronchial and pulmonary lymph nodes. The presence of gross pathological TB-like lesions was scored as previously described [27, 66]. Tissue samples were preserved in 10% phosphate-buffered formalin for 7 days before being embedded in paraffin wax. Four-micron sections were cut and stained with haematoxylin and eosin (H&E) or Ziehl-Neelsen staining for examination by light microscopy (at x100 magnification) to assess the number, developmental stage and distribution of each granuloma (types I-IV) [34, 35], the number of Langhans' cells as well as assessing the quantity and location of acid fast bacilli for each granuloma within the tissue section.

Statistical analysis

Results were plotted as mean ± SEM or SD and statistical analyses were performed in Microsoft Excel 2010 (Microsoft) and GraphPad Prism 8 (GraphPad Software Inc.). 2-tailed Student's t-tests were used to compare 2 groups and 1-way ANOVA with Tukey's multiple comparisons was used to compare 3 or more groups. A p-value is considered significant when < 0.05 and indicate as follow: *$p<0.05$; ** $p<0.01$; *** $p<0.001$; ns: not significant.

Ethical Statement

Holstein Friesian cows housed at the RVC Boltons Park Farm (Hertfordshire, UK) were used to obtain blood for PBMC isolation and subsequent Mϕ generation. Animals were held at the RVC under certificate of designation. Animals were dewormed regularly, checked regularly for the presence of bovine viral diarrhoea virus and bovine herpes virus, which both can infect bMϕ, leading to immunosuppression. Furthermore, all animals tested negative for bovine TB. All study cows received a physical examination, including assessment of the respiratory, cardiovascular, gastrointestinal, musculoskeletal, and reproductive systems, as well as skin, udder, and teats. The physical examination included BCS, pulse rate, respiration rate, and a rectal temperature conducted by a licensed veterinarian or trained designee approximately 7 d before their anticipated calving date. To avoid influences on cellular function through various stages in the reproductive cycle, animals used were age- and lactation-matched (2nd or 3rd lactation, respectively), and were in mid-lactation. All procedures were carried under Home Office Project licence (PPL7009059), after approval by the RVC's Ethics and Welfare Committee. Furthermore, handling of cows and blood sampling were conducted in accordance with EU legislation (Directive 2010/63/UE, related to the protection of animals used for scientific goals).

Acknowledgments

This work was supported by the Francis Crick Institute, which receives its core funding from Cancer Research UK, the UK Medical Research Council, and the Wellcome Trust and by the Biotechnology and Biological Sciences Research Council (BB/N004574/1), Science Foundation Ireland (SFI/15/IA/3154) and Wellcome Trust PhD studentship (109166/Z/15/A). We gratefully acknowledge Apoorva Bhatt for his critical advice and Chris Davies and Kat Pacey for technical assistance.

References

1. (WHO), W.H.O. (2019). Global TB report.
2. Davis, J.M., and Ramakrishnan, L. (2009). The role of the granuloma in expansion and dissemination of early tuberculous infection. Cell *136*, 37-49.
3. O'Garra, A., Redford, P.S., McNab, F.W., Bloom, C.I., Wilkinson, R.J., and Berry, M.P. (2013). The immune response in tuberculosis. Annu Rev Immunol *31*, 475-527.
4. Ulrichs, T., and Kaufmann, S.H. (2006). New insights into the function of granulomas in human tuberculosis. J Pathol *208*, 261-269.
5. Malone, K.M., and Gordon, S.V. (2017). Mycobacterium tuberculosis Complex Members Adapted to Wild and Domestic Animals. Adv Exp Med Biol *1019*, 135-154.
6. (WHO), W.H.O. (2005). Global TB Report.
7. Mableson, H.E., Okello, A., Picozzi, K., and Welburn, S.C. (2014). Neglected zoonotic diseases-the long and winding road to advocacy. PLoS Negl Trop Dis *8*, e2800.
8. Muller, B., Durr, S., Alonso, S., Hattendorf, J., Laisse, C.J., Parsons, S.D., van Helden, P.D., and Zinsstag, J. (2013). Zoonotic Mycobacterium bovis-induced tuberculosis in humans. Emerg Infect Dis *19*, 899-908.
9. Garnier, T., Eiglmeier, K., Camus, J.C., Medina, N., Mansoor, H., Pryor, M., Duthoy, S., Grondin, S., Lacroix, C., Monsempe, C., et al. (2003). The complete genome sequence of Mycobacterium bovis. Proc Natl Acad Sci U S A *100*, 7877-7882.
10. Malone, K.M., Farrell, D., Stuber, T.P., Schubert, O.T., Aebersold, R., Robbe-Austerman, S., and Gordon, S.V. (2017). Updated Reference Genome Sequence and Annotation of Mycobacterium bovis AF2122/97. Genome Announc *5*.
11. Malone, K.M., Rue-Albrecht, K., Magee, D.A., Conlon, K., Schubert, O.T., Nalpas, N.C., Browne, J.A., Smyth, A., Gormley, E., Aebersold, R., et al. (2018). Comparative 'omics analyses differentiate Mycobacterium tuberculosis and Mycobacterium bovis and reveal distinct macrophage responses to infection with the human and bovine tubercle bacilli. Microb Genom *4*.
12. Charlet, D., Mostowy, S., Alexander, D., Sit, L., Wiker, H.G., and Behr, M.A. (2005). Reduced expression of antigenic proteins MPB70 and MPB83 in Mycobacterium bovis BCG strains due to a start codon mutation in sigK. Mol Microbiol *56*, 1302-1313.
13. Gonzalo-Asensio, J., Malaga, W., Pawlik, A., Astarie-Dequeker, C., Passemar, C., Moreau, F., Laval, F., Daffe, M., Martin, C., Brosch, R., et al. (2014). Evolutionary history of tuberculosis shaped by conserved mutations in the PhoPR virulence regulator. Proc Natl Acad Sci U S A *111*, 11491-11496.
14. Said-Salim, B., Mostowy, S., Kristof, A.S., and Behr, M.A. (2006). Mutations in Mycobacterium tuberculosis Rv0444c, the gene encoding anti-SigK, explain high level expression of MPB70 and MPB83 in Mycobacterium bovis. Mol Microbiol *62*, 1251-1263.
15. Veyrier, F., Said-Salim, B., and Behr, M.A. (2008). Evolution of the mycobacterial SigK regulon. J Bacteriol *190*, 1891-1899.
16. Queval, C.J., Brosch, R., and Simeone, R. (2017). The Macrophage: A Disputed Fortress in the Battle against Mycobacterium tuberculosis. Front Microbiol *8*, 2284.
17. Cole, S.T., Brosch, R., Parkhill, J., Garnier, T., Churcher, C., Harris, D., Gordon, S.V., Eiglmeier, K., Gas, S., Barry, C.E., 3rd, et al. (1998). Deciphering the biology of Mycobacterium tuberculosis from the complete genome sequence. Nature *393*, 537-544.
18. Lerner, T.R., Borel, S., Greenwood, D.J., Repnik, U., Russell, M.R., Herbst, S., Jones, M.L., Collinson, L.M., Griffiths, G., and Gutierrez, M.G. (2017). Mycobacterium tuberculosis replicates within necrotic human macrophages. J Cell Biol *216*, 583-594.
19. Bussi, C., and Gutierrez, M.G. (2019). Mycobacterium tuberculosis infection of host cells in space and time. FEMS Microbiol Rev *43*, 341-361.

20. Lerner, T.R., Queval, C.J., Fearns, A., Repnik, U., Griffiths, G., and Gutierrez, M.G. (2018). Phthiocerol dimycocerosates promote access to the cytosol and intracellular burden of Mycobacterium tuberculosis in lymphatic endothelial cells. BMC Biol *16*, 1.
21. Schnettger, L., Rodgers, A., Repnik, U., Lai, R.P., Pei, G., Verdoes, M., Wilkinson, R.J., Young, D.B., and Gutierrez, M.G. (2017). A Rab20-Dependent Membrane Trafficking Pathway Controls M. tuberculosis Replication by Regulating Phagosome Spaciousness and Integrity. Cell Host Microbe *21*, 619-628 e615.
22. Gutierrez, M.G., Master, S.S., Singh, S.B., Taylor, G.A., Colombo, M.I., and Deretic, V. (2004). Autophagy is a defense mechanism inhibiting BCG and Mycobacterium tuberculosis survival in infected macrophages. Cell *119*, 753-766.
23. Watson, R.O., Bell, S.L., MacDuff, D.A., Kimmey, J.M., Diner, E.J., Olivas, J., Vance, R.E., Stallings, C.L., Virgin, H.W., and Cox, J.S. (2015). The Cytosolic Sensor cGAS Detects Mycobacterium tuberculosis DNA to Induce Type I Interferons and Activate Autophagy. Cell Host Microbe *17*, 811-819.
24. Watson, R.O., Manzanillo, P.S., and Cox, J.S. (2012). Extracellular M. tuberculosis DNA targets bacteria for autophagy by activating the host DNA-sensing pathway. Cell *150*, 803-815.
25. Collins, A.C., Cai, H., Li, T., Franco, L.H., Li, X.D., Nair, V.R., Scharn, C.R., Stamm, C.E., Levine, B., Chen, Z.J., et al. (2015). Cyclic GMP-AMP Synthase Is an Innate Immune DNA Sensor for Mycobacterium tuberculosis. Cell Host Microbe *17*, 820-828.
26. Wassermann, R., Gulen, M.F., Sala, C., Perin, S.G., Lou, Y., Rybniker, J., Schmid-Burgk, J.L., Schmidt, T., Hornung, V., Cole, S.T., et al. (2015). Mycobacterium tuberculosis Differentially Activates cGAS- and Inflammasome-Dependent Intracellular Immune Responses through ESX-1. Cell Host Microbe *17*, 799-810.
27. Villarreal-Ramos, B., Berg, S., Whelan, A., Holbert, S., Carreras, F., Salguero, F.J., Khatri, B.L., Malone, K., Rue-Albrecht, K., Shaughnessy, R., et al. (2018). Experimental infection of cattle with Mycobacterium tuberculosis isolates shows the attenuation of the human tubercle bacillus for cattle. Sci Rep *8*, 894.
28. Schnappinger, D., Ehrt, S., Voskuil, M.I., Liu, Y., Mangan, J.A., Monahan, I.M., Dolganov, G., Efron, B., Butcher, P.D., Nathan, C., et al. (2003). Transcriptional Adaptation of Mycobacterium tuberculosis within Macrophages: Insights into the Phagosomal Environment. J Exp Med *198*, 693-704.
29. Carr, M.D., Bloemink, M.J., Dentten, E., Whelan, A.O., Gordon, S.V., Kelly, G., Frenkiel, T.A., Hewinson, R.G., and Williamson, R.A. (2003). Solution structure of the Mycobacterium tuberculosis complex protein MPB70: from tuberculosis pathogenesis to inherited human corneal desease. J Biol Chem *278*, 43736-43743.
30. Park, S.Y., Jung, M.Y., and Kim, I.S. (2009). Stabilin-2 mediates homophilic cell-cell interactions via its FAS1 domains. FEBS Lett *583*, 1375-1380.
31. Nagai, S., Matsumoto, J., and Nagasuga, T. (1981). Specific skin-reactive protein from culture filtrate of Mycobacterium bovis BCG. Infect Immun *31*, 1152-1160.
32. Wiker, H.G., Lyashchenko, K.P., Aksoy, A.M., Lightbody, K.A., Pollock, J.M., Komissarenko, S.V., Bobrovnik, S.O., Kolesnikova, I.N., Mykhalsky, L.O., Gennaro, M.L., et al. (1998). Immunochemical characterization of the MPB70/80 and MPB83 proteins of Mycobacterium bovis. Infect Immun *66*, 1445-1452.
33. Smith, T. (1898). A Comparative Study of Bovine Tubercle Bacilli and of Human Bacilli from Sputum. J Exp Med *3*, 451-511.
34. Aranday-Cortes, E., Bull, N.C., Villarreal-Ramos, B., Gough, J., Hicks, D., Ortiz-Pelaez, A., Vordermeier, H.M., and Salguero, F.J. (2013). Upregulation of IL-17A, CXCL9 and CXCL10 in early-stage granulomas induced by Mycobacterium bovis in cattle. Transbound Emerg Dis *60*, 525-537.

35. Wangoo, A., Johnson, L., Gough, J., Ackbar, R., Inglut, S., Hicks, D., Spencer, Y., Hewinson, G., and Vordermeier, M. (2005). Advanced granulomatous lesions in Mycobacterium bovis-infected cattle are associated with increased expression of type I procollagen, gammadelta (WC1+) T cells and CD 68+ cells. J Comp Pathol *133*, 223-234.
36. Lun, S., Miranda, D., Kubler, A., Guo, H., Maiga, M.C., Winglee, K., Pelly, S., and Bishai, W.R. (2014). Synthetic lethality reveals mechanisms of Mycobacterium tuberculosis resistance to beta-lactams. mBio *5*, e01767-01714.
37. Pisu, D., Huang, L., Grenier, J.K., and Russell, D.G. (2020). Dual RNA-Seq of Mtb-Infected Macrophages In Vivo Reveals Ontologically Distinct Host-Pathogen Interactions. Cell Rep *30*, 335-350 e334.
38. Chen, E.H., and Olson, E.N. (2005). Unveiling the mechanisms of cell-cell fusion. Science *308*, 369-373.
39. Pereira, M., Petretto, E., Gordon, S., Bassett, J.H.D., Williams, G.R., and Behmoaras, J. (2018). Common signalling pathways in macrophage and osteoclast multinucleation. J Cell Sci *131*.
40. Vignery, A. (2005). Macrophage fusion: the making of osteoclasts and giant cells. J Exp Med *202*, 337-340.
41. Fleming, A., Sampey, G., Chung, M.C., Bailey, C., van Hoek, M.L., Kashanchi, F., and Hakami, R.M. (2014). The carrying pigeons of the cell: exosomes and their role in infectious diseases caused by human pathogens. Pathog Dis *71*, 109-120.
42. Giri, P.K., Kruh, N.A., Dobos, K.M., and Schorey, J.S. (2010). Proteomic analysis identifies highly antigenic proteins in exosomes from M. tuberculosis-infected and culture filtrate protein-treated macrophages. Proteomics *10*, 3190-3202.
43. Singh, P.P., LeMaire, C., Tan, J.C., Zeng, E., and Schorey, J.S. (2011). Exosomes released from M. tuberculosis infected cells can suppress IFN-gamma mediated activation of naive macrophages. PLoS One *6*, e18564.
44. Singh, P.P., Li, L., and Schorey, J.S. (2015). Exosomal RNA from Mycobacterium tuberculosis-Infected Cells Is Functional in Recipient Macrophages. Traffic *16*, 555-571.
45. Singh, P.P., Smith, V.L., Karakousis, P.C., and Schorey, J.S. (2012). Exosomes isolated from mycobacteria-infected mice or cultured macrophages can recruit and activate immune cells in vitro and in vivo. J Immunol *189*, 777-785.
46. Brooks, P.J., Glogauer, M., and McCulloch, C.A. (2019). An Overview of the Derivation and Function of Multinucleated Giant Cells and Their Role in Pathologic Processes. Am J Pathol *189*, 1145-1158.
47. McClean, C.M., and Tobin, D.M. (2016). Macrophage form, function, and phenotype in mycobacterial infection: lessons from tuberculosis and other diseases. Pathog Dis *74*.
48. Sakai, H., Okafuji, I., Nishikomori, R., Abe, J., Izawa, K., Kambe, N., Yasumi, T., Nakahata, T., and Heike, T. (2012). The CD40-CD40L axis and IFN-gamma play critical roles in Langhans giant cell formation. Int Immunol *24*, 5-15.
49. Yagi, M., Miyamoto, T., Sawatani, Y., Iwamoto, K., Hosogane, N., Fujita, N., Morita, K., Ninomiya, K., Suzuki, T., Miyamoto, K., et al. (2005). DC-STAMP is essential for cell-cell fusion in osteoclasts and foreign body giant cells. J Exp Med *202*, 345-351.
50. Silva Miranda, M., Breiman, A., Allain, S., Deknuydt, F., and Altare, F. (2012). The tuberculous granuloma: an unsuccessful host defence mechanism providing a safety shelter for the bacteria? Clin Dev Immunol *2012*, 139127.
51. Milde, R., Ritter, J., Tennent, G.A., Loesch, A., Martinez, F.O., Gordon, S., Pepys, M.B., Verschoor, A., and Helming, L. (2015). Multinucleated Giant Cells Are Specialized for Complement-Mediated Phagocytosis and Large Target Destruction. Cell Rep *13*, 1937-1948.
52. Lay, G., Poquet, Y., Salek-Peyron, P., Puissegur, M.P., Botanch, C., Bon, H., Levillain, F., Duteyrat, J.L., Emile, J.F., and Altare, F. (2007). Langhans giant cells from M. tuberculosis-induced human granulomas cannot mediate mycobacterial uptake. J Pathol *211*, 76-85.

53. Chen, Y., Chao, Y., Deng, Q., Liu, T., Xiang, J., Chen, J., Zhou, J., Zhan, Z., Kuang, Y., Cai, H., et al. (2009). Potential challenges to the Stop TB Plan for humans in China; cattle maintain M. bovis and M. tuberculosis. Tuberculosis (Edinb) *89*, 95-100.
54. Ocepek, M., Pate, M., Zolnir-Dovc, M., and Poljak, M. (2005). Transmission of Mycobacterium tuberculosis from human to cattle. J Clin Microbiol *43*, 3555-3557.
55. Palaniyandi, K., Kumar, N., Veerasamy, M., Kabir Refaya, A., Dolla, C., Balaji, S., Baskaran, D., Thiruvengadam, K., Rajendran, A., Narayanan, S., et al. (2019). Isolation and comparative genomics of Mycobacterium tuberculosis isolates from cattle and their attendants in South India. Sci Rep *9*, 17892.
56. Ameni, G., Vordermeier, M., Firdessa, R., Aseffa, A., Hewinson, G., Gordon, S.V., and Berg, S. (2011). Mycobacterium tuberculosis infection in grazing cattle in central Ethiopia. Vet J *188*, 359-361.
57. Shrivastava, P., and Bagchi, T. (2013). IL-10 modulates in vitro multinucleate giant cell formation in human tuberculosis. PLoS One *8*, e77680.
58. Palmer, M.V., Thacker, T.C., and Waters, W.R. (2016). Multinucleated giant cell cytokine expression in pulmonary granulomas of cattle experimentally infected with Mycobacterium bovis. Vet Immunol Immunopathol *180*, 34-39.
59. Werling, D., Hope, J.C., Howard, C.J., and Jungi, T.W. (2004). Differential production of cytokines, reactive oxygen and nitrogen by bovine macrophages and dendritic cells stimulated with Toll-like receptor agonists. Immunology *111*, 41-52.
60. Wisniewski, J.R., Zougman, A., Nagaraj, N., and Mann, M. (2009). Universal sample preparation method for proteome analysis. Nat Methods *6*, 359-362.
61. Cox, J., and Mann, M. (2008). MaxQuant enables high peptide identification rates, individualized p.p.b.-range mass accuracies and proteome-wide protein quantification. Nat Biotechnol *26*, 1367-1372.
62. Cox, J., Neuhauser, N., Michalski, A., Scheltema, R.A., Olsen, J.V., and Mann, M. (2011). Andromeda: a peptide search engine integrated into the MaxQuant environment. J Proteome Res *10*, 1794-1805.
63. Cox, J., Hein, M.Y., Luber, C.A., Paron, I., Nagaraj, N., and Mann, M. (2014). Accurate proteome-wide label-free quantification by delayed normalization and maximal peptide ratio extraction, termed MaxLFQ. Mol Cell Proteomics *13*, 2513-2526.
64. Tyanova, S., Temu, T., Sinitcyn, P., Carlson, A., Hein, M.Y., Geiger, T., Mann, M., and Cox, J. (2016). The Perseus computational platform for comprehensive analysis of (prote)omics data. Nat Methods *13*, 731-740.
65. Whelan, A., Court, P., Xing, Z., Clifford, D., Hogarth, P.J., Vordermeier, M., and Villarreal-Ramos, B. (2012). Immunogenicity comparison of the intradermal or endobronchial boosting of BCG vaccinates with Ad5-85A. Vaccine *30*, 6294-6300.
66. Vordermeier, H.M., Chambers, M.A., Cockle, P.J., Whelan, A.O., Simmons, J., and Hewinson, R.G. (2002). Correlation of ESAT-6-specific gamma interferon production with pathology in cattle following Mycobacterium bovis BCG vaccination against experimental bovine tuberculosis. Infect Immun *70*, 3026-3032.

Figure Legends

Fig. 1: Mtb and Mbv differentially replicate and localise within human or bovine macrophages. (A) Confocal images of monocyte-derived GM-CSF differentiated-human or bovine Mϕ (hMϕ or bMϕ) infected with RFP-expressing *M. tuberculosis* H37Rv (Mtb-RFP) or *M. bovis* (Mbv-RFP) for 2, 24 and 72 h. Brightfield was used to

visualize the cells. Cell nuclei were stained with DAPI (blue) and bacteria-RFP are visualized in red. Scale bar: 20 µm. **(B** and **C)** Quantification of intracellular growth expressed in bacteria area (µm^2) per infected cell of Mtb-RFP and Mbv-RFP within hMϕ **(B)** and bMϕ **(C)**. (**D** and **E**) Electron microscopy images of hMϕ (**D**) and bMϕ (**E**) infected with Mtb or Mbv for 24 h. Asterisks mark the intracellular bacteria. Images were selected to illustrate free cytosolic bacteria (left-hand panels), phagosomal bacteria (middle panels) and bacteria surrounded by multiple membranes (right-hand panels). Scale bar, 200 nm. (**F**) Quantification by stereology of the proportion of bacteria contained in each compartment. Black represents the proportion of cytosolic bacteria; green, the proportion of single membrane bound bacteria, and grey, the bacteria surrounded by multiple membranes. (**G**) Quantification by RT-qPCR of the relative fold change mRNA expression of interferon-β (*IFN- β*) in hMϕ (**left graph**) and bMϕ (**right graph**) infected with Mtb or Mbv for 24 h. Data are normalized to Mtb. (Housekeeping gene used: *GAPDH*).

Fig. 2: Mbv specifically induces the formation of MNCs in bMϕ. (**A**) Fluorescence confocal images of bMϕ infected with Mtb-RFP or Mbv-RFP for 24 h. Non-infected cells (NI) were used as a control. The bacteria are visualized in red, the cell actin cytoskeleton is in white (phalloidin-488) and cell nuclei (DAPI) in cyan. Arrows highlight the cells containing 2 or more nuclei, corresponding to multinucleated cells (MNCs). Scale bar, 50 µm. (**B**) Quantification of the percentage of MNCs in bMϕ infected with Mtb-RFP or Mbv-RFP for 24 hours. Non-infected cells (NI) were used as a control. Each dot represents one donor tested. (**C**) Quantification of the percentage of MNCs in hMϕ infected with Mtb-RFP or Mbv-RFP for 24 h. Non-infected cells (NI) were used as a control. (**D**) Electron microscopy image of an uninfected bystander-MNC containing four distinct nuclei. The images displayed on the right side correspond to the magnification of each region (a-c) delimited by black squares in the main image. Scale bar are D: 40 µm; D^a: 2 µm; D^b: 2 µm; D^c: 1 µm. (**E**) Maximum projection (14 Z-stacks with an interval of 0.8 µm) from confocal images of bovine MNCs without intracellular Mbv-RFP (Byst-MNC) or containing intracellular Mbv-RFP (Mbv-MNC). In the latter image, the presence of intracellular bacteria is highlighted in the region delimited by a white square, magnified in the right corner. Bacteria are visualized in red, the cells with brightfield image, and nuclei in cyan. A dashed line delimits the edge of MNCs. (**F**)

Quantification of the percentage of bystander and Mbv-MNCs in the Mbv-infected bMϕ population for two independent donors. Each bar chart represents the total MNCs population (100%); in black is percentage of Mbv-infected MNCs, and in grey the percentage of uninfected bystander-MNCs.

Fig. 3: Secreted bacterial MPB70 contributes to MNCs formation in bMϕ.

(**A**) Culture filtrate from Mbv wild-type (WT), Mbv ΔMPB70, Mbv ΔMPB70/MPB70 (Mbv-Compl.) were assessed for immuno-labelling of MPB70 (23 kDa). Immuno-labelling of Ag85 (38 kDa) was used as gel loading control (**B**) Fluorescence confocal images of bMϕ infected Mbv WT, Mbv ΔMPB70, Mbv-Compl. for 24 h. Uninfected cells had been used as a negative control. Cell nuclei are stained with DAPI (cyan) and actin is visualized in grey. Yellow arrows point the multi-nucleated cells. Scale bar, 50 µm (**C**) Quantification of MNCs from each experiment displayed in **B**. Graph represents the quantification of MNCs for each condition tested where each dot represents one bovine donor. Data shown are representative of four biological repeats.

Fig. 4: Extracellular vesicles produced by Mbv-infected bMϕ induce cell multi-nucleation.

(**A**) A total of 192 proteins were determined to be differentially regulated using an ANOVA and Tukey's post-hoc test in the secretome of infected bMϕ and sorted according to Gene Ontology Cellular Component (GOCC). (**B** and **C**) List of 27 proteins differentially expressed in the secretome of Mtb-infected or Mbv-infected bMϕ clustered into 3 groups: extracellular vesicles, membrane trafficking and cell adhesion or others. The $\log_2$ fold change Mtb or Mbv, both normalised to uninfected (NI), samples are displayed in (**B**) and the $\log_2$ fold change Mbv/Mtb is displayed in (**C**). Proteomics data were obtained from 3 independent experiments carried out with 3 different bovine donors. (**D**) EVs purification procedure summarized in 3 steps. (**E**) Electron microscopy micrographs of EVs-enriched fraction. The white arrows show the extracellular vesicles. Scale bar: 0.1 µm. (**F**) Fluorescence confocal images of naïve bMϕ stimulated for 24 hours with EVs-enriched fraction from uninfected (NI), Mtb-infected or Mbv-infected bMϕ. Cell nuclei are stained with DAPI (cyan) and actin is visualized in grey. Yellow arrows point the MNCs. Scale bar: 50 µm (**G**) Quantification of MNCs after bMϕ stimulation with EVs-enriched fractions. The graph

represents the quantification of MNCs for each condition tested where each dot represents one bovine donor. Data are representative of 4 independent experiments.

Fig. 5: Granulomas from Mbv-infected cows contain a higher number of MNCs than Mtb-infected cows. (**A, left image**) Histological Haematoxylin and Eosin (H&E) staining of granulomatous lesions in thoracic lymph nodes of cows challenged for 10 weeks with Mtb H37Rv strains. Scale bar, 200 µm. (**A, right image**) higher magnification of multinucleated giant cells (white square). Scale bar, 50 µm. (**B**, **left image**) H&E staining of granulomatous lesions in thoracic lymph nodes of cows challenged for 6 weeks with Mbv AF2122/97. Scale bar, 200 µm. (**B**, **right image**) higher magnification of multinucleated giant cells (white square). Scale bar, 50 µm. (**A** and **B**) Granulomas are classified from early stage of maturation (type I and II) to late granulomas (type III and IV) (**C**) Quantification of the number of granulomas counted for each condition. (**D**) Quantification of bacterial load in each granuloma based on acid fast staining of the tissue section and expressed as the mean Acid Fast Bacilli (AFB) ± SEM. (**E**) Quantification of the number of MNCs per granuloma ± SEM.

Supplementary Figures

Fig. S1: Physiological and morphological differences between GM-CSF-derived human and bovine macrophages.

(**A**) hMϕ were infected with Mtb-RFP or Mbv-RFP at an MOI of 10, whereas bMϕ were infected at an MOI of 1. Intracellular bacteria were quantified based on intracellular RFP signal and expressed in bacteria area per infected cells. Each dot represents the average of 10 fields from 2 independent experiments (also with different donors). **(B)** Evolution of the number of hMϕ during the course of infection (2 to 120 hours post-infection). **(C)** Evolution of the number of bMφ during the course of infection (2 to 72 hours post-infection). (**D**) Left panel: Confocal images of hMϕ infected with Mtb-RFP or Mbv-RFP after 5 days of infection. Brightfield was used to visualize the cells. Bacteria are visualized in red, cell nuclei were stained with DAPI (blue) and nuclei from dead cells in green. Scale bar: 20 µm. Right panel: Quantification of the level of cytotoxicity based on Green Live/Dead stain; uninfected. Non-infected cells (NI) were used as a control, n represents the number of cells analysed. **(E)** Left panel: Confocal images of hMϕ infected with Mtb-RFP or Mbv-

RFP for 2 hours or 8 days. Actin (in green) was used to visualize the cells. Cell nuclei were stained with DAPI (blue) and bacteria-RFP are visualized in red. Scale bar: 20 µm. Right panel: quantification of intracellular growth expressed in bacteria area (μm^2) per hMϕ. Data are representative of 2 independent experiments. (**F**) Representative electron microscopy images of hMϕ and bMϕ. Scale bar: 5 µm (**G**) Representative confocal images of hMϕ or bMϕ fluorescently stained for the late endosomal marker Lamp-1. The regions in the white squares are highlighted on the right-hand side of the micrograph.

Fig. S2: Differential intracellular trafficking between Mtb and Mbv. hMϕ or bMϕ infected with Mtb-RFP or Mbv-RFP (**A**, **B**, **E** and **F**) or Mtb-GFP or Mbv-GFP (**B** and **C**) for 24 h. Samples were fixed and fluorescently stained for the late endosomal marker Lamp-1 (**A** and **B**), for the pH sensitive dye LysoTracker DN99 Red (LTR) (**C** and **D**) and for the autophagic marker LC3B (**E** and **F**). For each fluorescent confocal image, the cell nuclei were stained with DAPI. Positive association of bacteria with the different markers, delimited by a white square, are magnified and displayed at the top right corner and the right-hand side of each image. Scale bars represent 10 µm. Graphs represent the quantification of the marker association with Mtb or Mbv ± SEM from three independent experiments. Each dot represents the mean relative fluorescent intensity of the cellular marker with a single or distinct bacteria group. The population within each dotted red box corresponds to the percentage (± STD) of bacteria positive for the marker tested.

Fig. S3: Mbv induces multinucleation of bMϕ. (**A**) Fluorescence confocal images of bMϕ infected with Mtb-RFP, Mbv-RFP or PFA-killed-Mbv-RFP for 24 h. Non-infected cells (NI) were used as a control. The bacteria are visualized in red, the cells-actin cytoskeleton is in white (phalloidin-488) and cell nuclei (DAPI) in cyan. The white square represents a region of interest magnified below each image. Arrows highlight the MNCs containing 2 or more nuclei. Scale bar, 40 µm. (**B**) Quantification of the percentage of MNCs in bMϕ for each condition. Data are representative of two independent biological repeats, each carried out in duplicate. (**C**) Electron microscopy image of Mbv-induced bovine MNCs containing three or six distinct nuclei (black arrows). Scale bar, 10 µm. (**D**) Supernatant transfer assay from, bMϕ infected with Mtb, Mbv, PFA-killed Mbv, or hMϕ infected with Mtb or Mbv for 24

h, onto naïve bMϕ. Graph represents the number of MNC formed in cultures of naïve bMϕ following the addition of 400 µl of supernatant derived from cultures of bMϕ infected with Mbv or Mtb (**E**) Supernatant transfer assay from hMϕ infected with Mtb, Mbv, PFA-killed Mbv, or bMϕ infected with Mtb or Mbv for 24 h, onto naïve hMϕ. The graph represents the quantification of MNCs for each condition tested. (**D** and **E**) Data are representative of 2 independent experiments, each carried out in duplicates.

Fig. S4: Cloning *M. bovis* MPB70 mutants and secretome analysis: (A) Genetic arrangement *M. bovis* wild-type (WT) and *M. bovis* mpb70 knock-out (Δmpb70) strains. **(B)** Genetic organisation of *dipZ-mpb70* genes and primer locations **(C)** Characterisation of *M. bovis* mutants by PCR. Deletion of mpb70 and maintenance of *dipZ* in *M. bovis* Δmpb70 and complemented compared to WT. *dipZ* is amplified in all the strains. *mpb70* (244 bp) was amplified in the WT strain but not in Δmpb70 and complemented strains. The PCR with a forward primer in *dipZ* and reverse primer in mpb70 gave the expected amplification of a 370 bp product for WT, but was absent in Δmpb70. Its absence from the complemented Δmpb70/mpb70 (Compl) strain, confirms that the location of *mpb70* gene, carried by the replicative plasmid pEW70c2, is distal to the wild type chromosomal location. **(D)** Western immunoblot for detection of MPB70 in the supernatant of the Mbv WT, Δmpb70 and complemented (Mbv-Compl) strains. Each sample was analysed in duplicate. A 23 kDa band corresponding to MPB70 was detected for the WT and complemented strain but not for Δmpb70 strain. (**E**) Principal component analysis of secretome samples. Distinct clusters of sample groups are observed that indicate high reproducibility between replicates and major protein expression differences between the samples analysed. (**F**) Unsupervised hierarchical clustering of secretome samples. Distinct clusters of sample groups indicate high reproducibility of replicates and distinct protein expression differences between the samples. Two major clusters are observed with uninfected controls clustering separately from mycobacterial-infected samples. Protein groups with lower abundance (i.e. lower LFQ intensity) are in purple and protein groups with higher abundance are in orange.

Table S1: Proteins secreted by bMϕ during infection with Mtb or Mbv.

1170 **Table S2:** Mass spectrometric raw data of the secretome of non-infected (NI), Mtb-
1171 or Mbv-infected bMϕ.

Figure 1

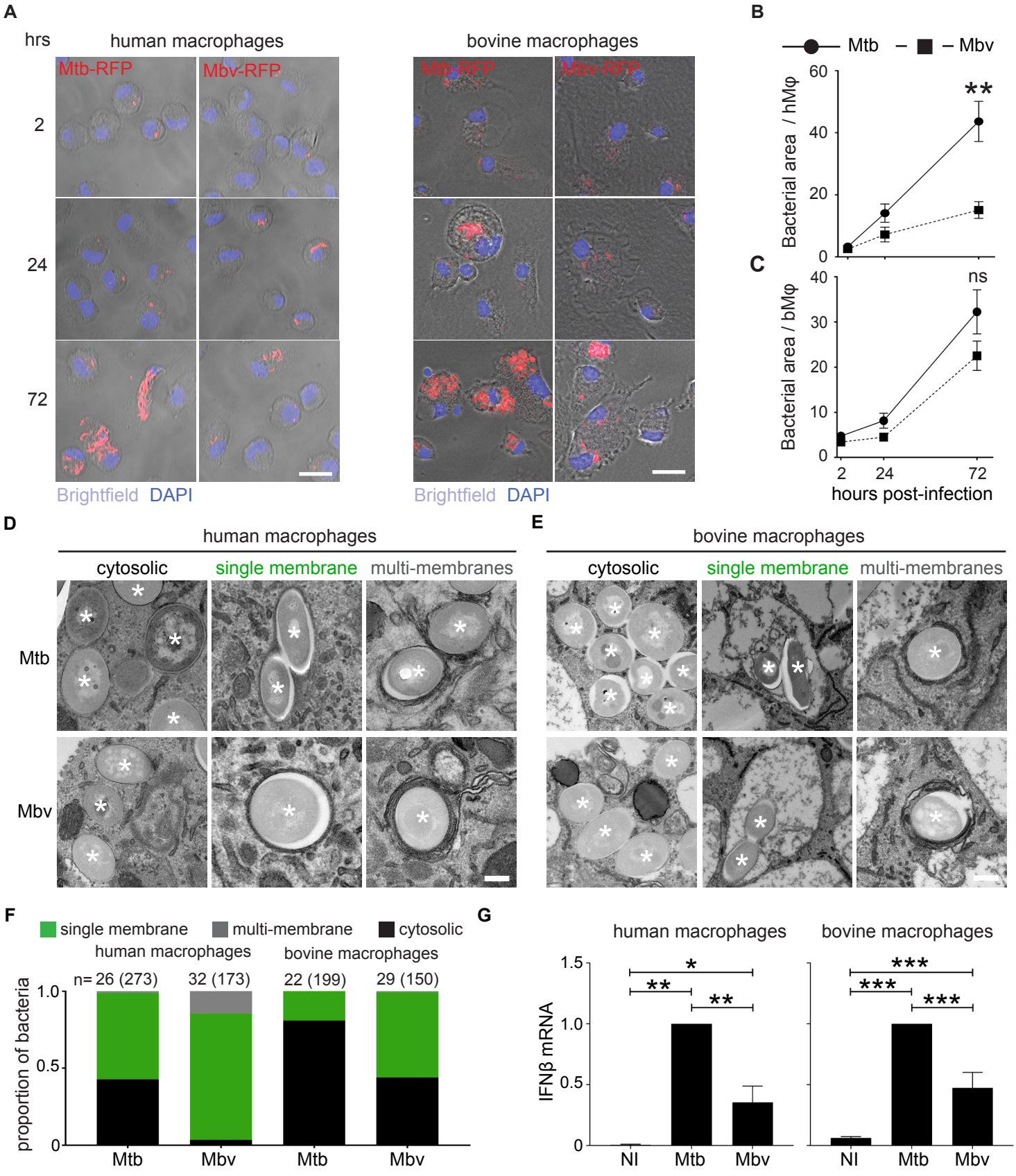

Figure 2

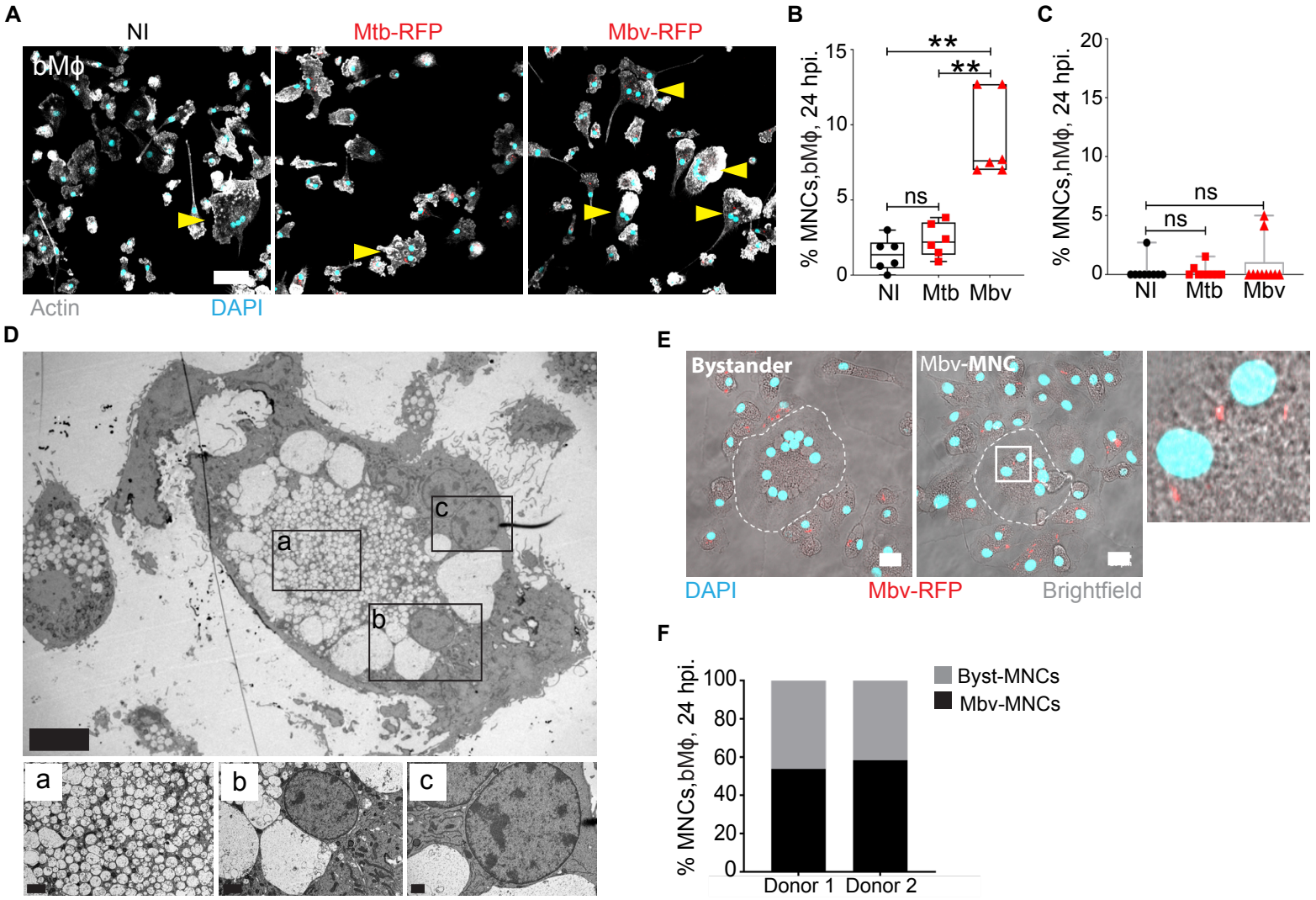

Figure 3

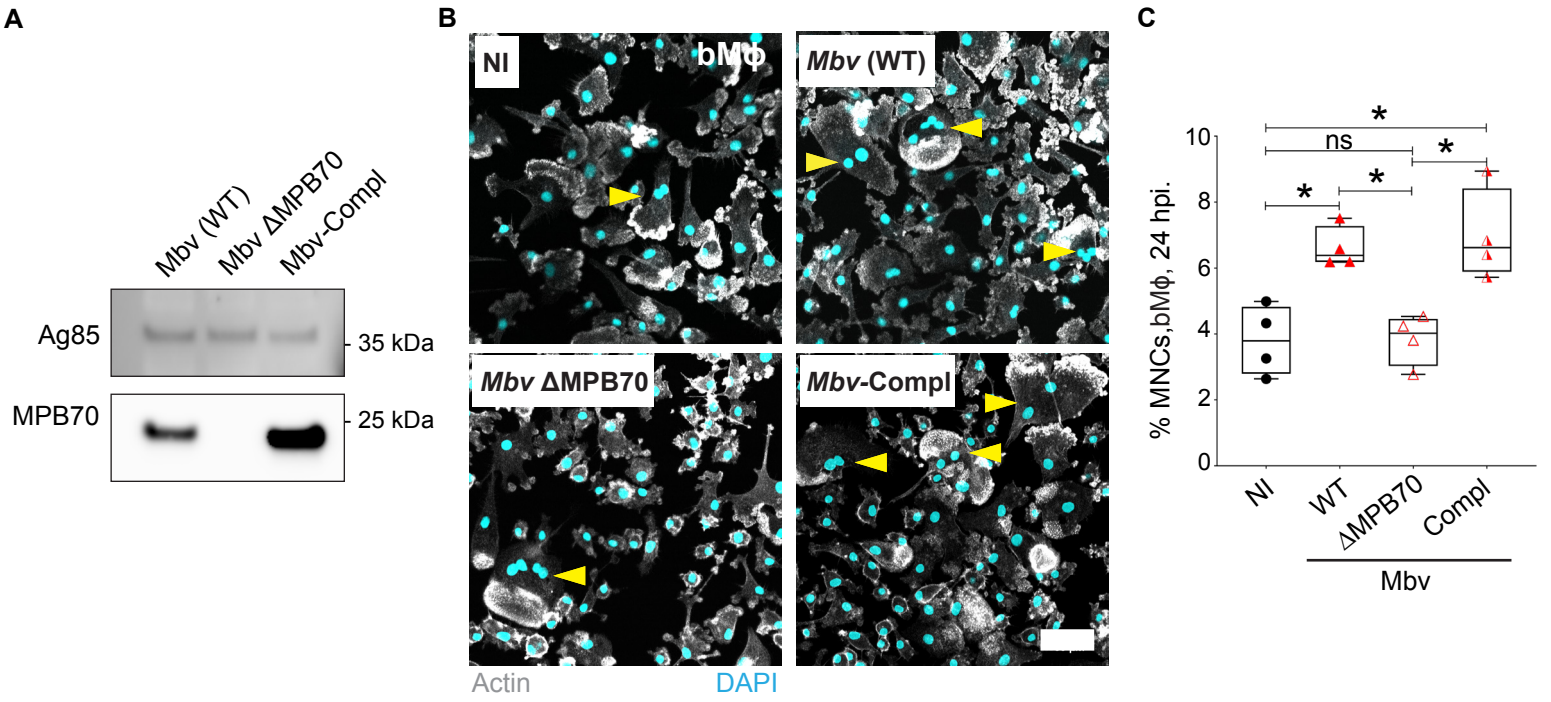

Figure 4

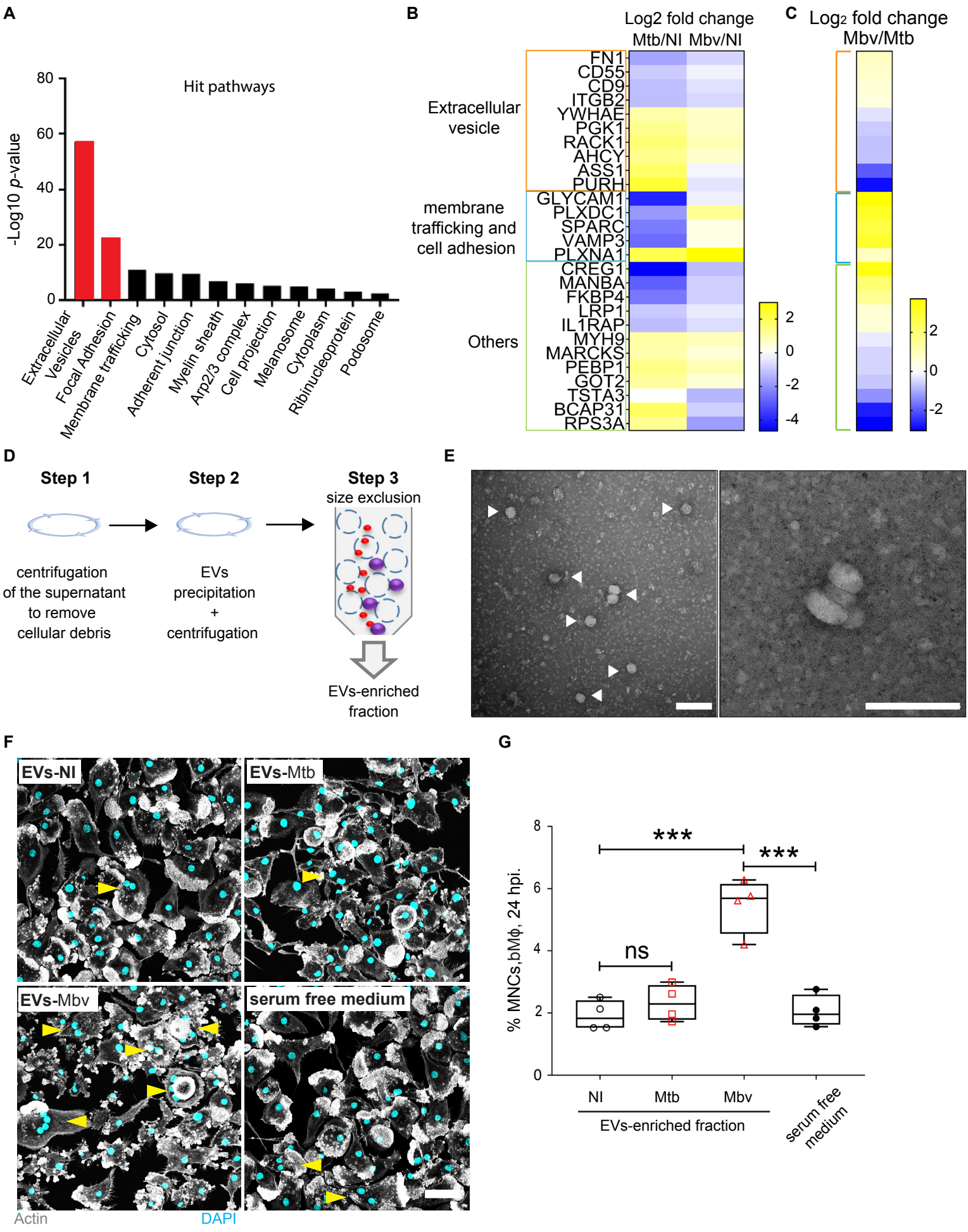

Figure 5